Geophys. J. Int. (2009) **178,** 1597–1613 doi: 10.1111/j.1365-246X.2009.04246.x

Estimation of non-linear site response in a deep Alpine valley

D. Roten,[1,*] D. Fäh,[1] L. F. Bonilla,[2] S. Alvarez-Rubio,[1,3] T. M. Weber[4,†] and J. Laue[4]

[1] *ETH Zurich, Institute of Geophysics, Sonneggstrasse* 5, 8092 *Zürich, Switzerland. E-mail: droten@sciences.sdsu.edu*
[2] *Institut de Radioprotection et de Súreté Nucléaire,* BP 17, *Fontenay-aux-Roses, Cedex, France*
[3] *UPM, EUITI, Dpto Matem'tica Aplicada,* 28012 *Madrid, Spain*
[4] *ETH Zurich, Institute for Geotechnical Engineeering,* 8093 *Zürich, Switzerland*

Accepted 2009 May 12. Received 2009 May 12; in original form 2008 July 21

SUMMARY

We simulate non-linear behaviour of soils during strong ground motion in the Rhône valley in southern Switzerland. Previous studies of the site response using weak ground motion, ambient noise and linear 3-D FD simulations suggest that the 2-D structure of the basin will lead to amplification factors of up to 12 in the frequency band between 0.5 and 10 Hz.

To estimate the importance of non-linear soil behaviour during strong ground motion in the Rhône valley we simulate the response of a superficial soft layer with a fully non-linear 1-D finite difference code. The non-linear wave propagator is based on an effective stress constitutive soil model capable of predicting pore pressure evolution due to shear. We determine the required dilatancy parameters from laboratory analysis of soil samples using cyclic triaxial tests. In order to include the effect of the strong 2-D structure in our non-linear analysis synthetic seismograms are convolved with the transfer function of the basin and then propagated through a 1-D non-linear layer.

We find that reduced amplification due to soil non-linearity can be expected at rock accelerations above 0.5 ms^{-2}, and that de-amplification occurs at ground motion levels of approximately 2 ms^{-2}.

Nevertheless, the spectral accelerations simulated for the valley centre are still exceeding the design spectra at about 0.5 Hz for magnitudes above 6.0, which reflects the strong amplification of ground motion by the deep 2-D resonance of the basin. For frequencies above 1 Hz the design spectra are generally in agreement with the strongest simulated accelerations.

We evaluate the occurrence of soil failure using the 5 per cent strain criterion as a function of hypocentral distance and magnitude. Results confirm observations of liquefaction reported after the 1855 M_w 6.4 earthquake of Visp, and they suggest that soil liquefaction may occur at distances beyond those predicted by empirical relations in the valley. Near the basin edge, however, the simulated liquefaction occurrence agrees with the empirical relations. These results suggest that the response of the whole structure needs to be simulated in order to estimate the non-linear seismic response of complex basins like the Rhône valley.

Key words: Earthquake ground motions; Site effects; Computational seismology; Wave propagation.

1 INTRODUCTION

It is generally accepted that soft, unconsolidated deposits tend to amplify earthquake ground motion and increased damage associated with such soft soils has been observed during many devastating earthquakes.

A common seismological approach to quantify soft soil amplification consists in recording weak ground motion from local earthquakes on both rock and soft soil sites. These records are used to compute site-to-reference spectral ratios, on the basis of which frequencies of amplification are estimated and the amount of amplification is quantified. However, the validity of weak motion records to predict the site response during strong ground motion is questionable, because soft soils may exhibit non-linear behaviour during strong earthquakes.

In the last decades the seismological community has become increasingly aware of the importance of non-linear site response (e.g. Beresnev & Wen 1996; Hartzell *et al.* 2004; Bonilla *et al.* 2005). Basically non-linear soil behaviour marks the breakdown of the linear relationship between stress and strain. The shear modulus is reduced and damping increased at high-strain levels. This increased

*Now at: San Diego State University, Department of Geological Sciences, San Diego, CA, USA.
†Now at: Studer Engineering, Thujastrasse 4, 8038 Zürich, Switzerland.

damping may reduce the amplification of strong ground motion on soft soil, and even lead to a de-amplification compared to a bedrock site. Additionally, the reduced shear wave velocity reduces the resonant frequency of the soft layer. Observational evidence for this type of soil response was, among others, found in records of the 1989 Loma Prieta earthquake (Darragh & Shakal 1991), the 1994 Northridge earthquake (Field *et al.* 1997) and records from vertical arrays in Taiwan (Wen *et al.* 1994). A comprehensive review of observed non-linear soil behaviour can be found in Beresnev & Wen (1996).

However, non-linearity does not necessarily involve reduced amplification or de-amplification. Recent laboratory and field data suggest that cohesionless soils may momentarily recover their shear strength during strong ground motion due to their dilatant nature (Bonilla *et al.* 2005). This effect produces large deformations and spiky shear stresses, and the resulting high-amplitude spikes in surface ground motion present significant accelerations.

Records of such spiky accelerograms at the Kushiro Port (Iai *et al.* 1995) and Wildlife Refugee (Holzer *et al.* 1989) vertical arrays demonstrate that these spikes are related to the soft unconsolidated soil. Bonilla *et al.* (2005) simulated the soil response of Kushiro Port and Wildlife Refugee using a fully non-linear 1-D propagator, and obtained waveforms with high-frequency peaks riding on a low frequency carrier, similar to the observations. These findings demonstrate the complexity of soft soil response at high-strain levels.

In this paper, we analyse the importance of non-linear site effects for the Rhône valley in southern Switzerland. In a previous study, we estimated the seismic response of the Rhône basin using weak ground motion recorded on a temporary array in the city of Sion (Roten *et al.* 2008). Site-to-reference spectral ratios revealed an amplification level of up to 12 at the fundamental frequency of the basin between 0.5 and 0.6 Hz, which can be reproduced by 3-D numerical simulations using a detailed velocity model of the Sion basin. At some stations, amplifications of up to 20 were observed at higher frequencies of 8–10 Hz.

The Rhône valley is located in the area of the highest seismicity in Switzerland, and the region was struck by several large earthquakes with magnitudes above 6 in the last decades, for example, the 1946 M 6.1 earthquake of Sierre and the 1855 M 6.4 earthquake of Visp. Since the last large earthquake, extensive development has taken place especially on the soft unconsolidated Rhône deposits. The levels of amplification observed from weak ground motion would lead to strong accelerations and significant damage during future M 6 events. In order to prepare for future earthquakes engineers and seismologists need to know how non-linear soil-behaviour will influence strong ground motion in the Rhône valley. Evidence of non-linear soil response, such as cracks in the ground and lateral spreading, were observed at several sites after the 1946 and 1855 earthquakes (Fritsche *et al.* 2006).

In this study, we will assess the importance of non-linear soil behaviour for the area using laboratory data of soil samples and numerical simulations with a fully non-linear 1-D propagator (Bonilla *et al.* 2005). We will estimate at what level of rock acceleration reduced amplification, or even de-amplification, may be expected. We will also assess how non-linear soil response may affect signals recorded on the surface, especially considering the spiky waveforms discussed above.

2 GEOPHYSICAL SETTING

The Rhône valley is a deeply eroded basin in the canton Valais in southern Switzerland (Fig. 1). A few high-resolution seismic profiles (Besson *et al.* 1993; Pfiffner *et al.* 1997) and gravimetric surveys (Rosselli 2001) have been performed across the basin to examine the structure of the unconsolidated sedimentary fill. Below the city of Sion, the basin is about 500 m deep. Array measurements of ambient noise were conducted at several places in the Rhône valley to constrain the shear wave velocity of the sedimentary fill, especially in the Sion area (Roten & Fäh 2007).

These ambient noise array measurements revealed a shallow superficial layer with shear wave velocities between 150 and 250 ms^{-1} at most sites. Below this layer shear wave velocities range between 320 and 500 ms^{-1}, and velocities of up to 1000 ms^{-1} were reported for the lowermost layer. At most recorded sites, including Martigny, Sion and Visp, a shallow layer with shear wave velocities between 150 and 250 ms^{-1} was resolved. Fig. 2 shows an example of inversion results obtained from an array measurement of ambient noise near Visp. The *geopsy* (available at: http://www.geopsy.org) program package (Wathelet *et al.* 2004) was used for the frequency–wavenumber processing and the inversion of the dispersion curve. The uppermost low-velocity layer is about 30 m thick at this site, with velocities between 200 and 250 ms^{-1}. Below this layer, the

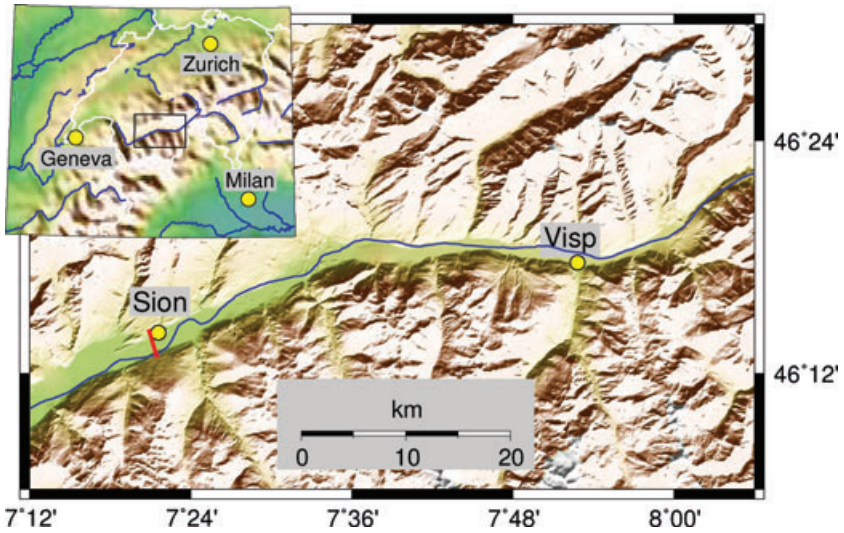

Figure 1. Map of the Rhône valley. Soil samples were taken in Visp. The red bar near Sion shows the location of the cross-section shown in Fig. 3(a).

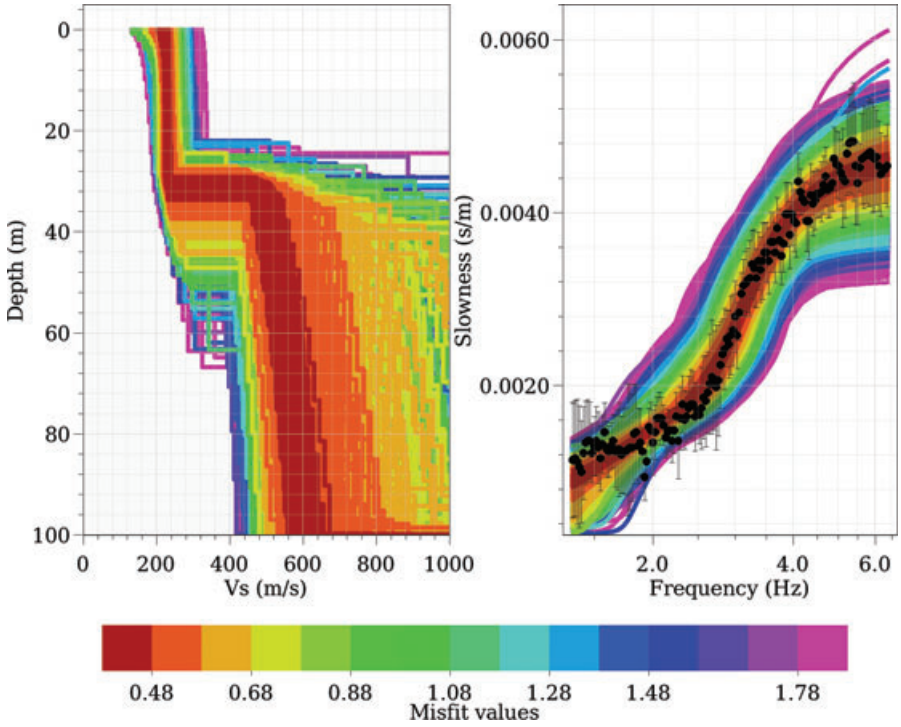

Figure 2. Inversion results from array measurement of ambient noise near Visp. Right-hand panel: recorded and modelled dispersion curves. Left-hand panel: shear wave velocities of obtained models. Results with lowest misfit are plotted darkred.

shear velocity increases to more than 500 ms^{-1}, which is similar to the values recorded at other sites. This low velocity layer is also encountered in borehole logs from various places in the valley. It consists of saturated sands and gravels from the Rhône, as most of the valley was a floodplain before the river was channelled in the 19th century.

To characterize the geotechnical properties of this low-velocity layer, a set of samples was taken from an excavation pit in Visp at a depth of 6 m. We conducted a series of laboratory tests on these samples to estimate the parameters for the non-linear analysis.

3 METHOD

We assume that only the uppermost low-velocity layer exhibits non-linear behaviour, and use linear analysis for the remaining sedimentary fill down to the bedrock. We will use the 'NOAH' program (Bonilla *et al.* 2005), a non-linear 1-D finite difference code, which incorporates the strain space multishear mechanism model (Towhata & Ishihara 1985). 'NOAH' computes the non-linear wave propagation in water saturated soil deposits subjected to vertically incident SH ground motion. However, we chose not to use 1-D analysis for the whole sedimentary fill from previous experience. Both results from ambient noise (Roten *et al.* 2006) and weak motion records (Roten *et al.* 2008) show that the deep response of the Rhône basin is caused by 2-D resonance, which causes higher amplification than 1-D response. In order to analyse both the 2-D response of the deep basin and the non-linear response of the soft superficial layer, we combine results of 2-D numerical simulations for a cross-section through the valley with the 1-D non-linear FD code.

3.1 Combined 2-D linear and 1-D non-linear simulations

Fig. 3(a) shows the cross-section that was used for the 2-D simulations. Although the soil samples were taken in Visp, we will model the response of the Sion basin, because our previous study of weak ground motion focused on the Sion area and no detailed velocity model has yet been developed for Visp. The cross-section was extracted from a 3-D velocity model created for the central Valais region (Roten *et al.* 2008) and does not contain the low-velocity layer. Table 1 shows the physical properties of the individual layers in the velocity model. We will assume that the non-linear properties of the soil are the same in Sion and Visp, since no samples for Sion are available. The depth of the non-linear layer was set to 10 m to match observations made in the Sion area (Roten & Fäh 2007).

Using the 2-D profile in Fig. 3(a), we simulated a vertically incident SV wave with the Direct Boundary Element Method (DBEM, Álvarez-Rubio *et al.* 2004; Álvarez-Rubio *et al.* 2005). Since 'NOAH' models the SH case we only use the horizontal component of the DBEM synthetics, which is oriented in the direction perpendicular to the valley axis as the DBEM is restricted to the in-plane (P–SV) case (Álvarez-Rubio *et al.* 2004). We computed the transfer function between a station on bedrock and on the soil surface in the valley centre (Fig. 3a) for the horizontal component. Fig. 3(c) shows the absolute value of the obtained transfer function. The 2-D resonance creates a dominant peak at about 0.5 Hz, and a further peak appears at 2 Hz.

The greatest uncertainty in our analysis comes from the input ground motion at the bottom of the velocity model. For the historical earthquakes reported in the Valais, the originating fault and source mechanisms are not known, and we have no indication about where a future earthquake will happen. We can, therefore, not simulate the input ground motion with a physics-based model but have to use a stochastic method instead.

To generate a set of non-stationary synthetic seismograms we used the empirical method proposed by Pousse *et al.* (2006), which represents an improved version of a stochastic model developed by Sabetta and Pugliese (1996). This method models the acceleration time histories using time envelopes for the *P, S* and coda waves. The

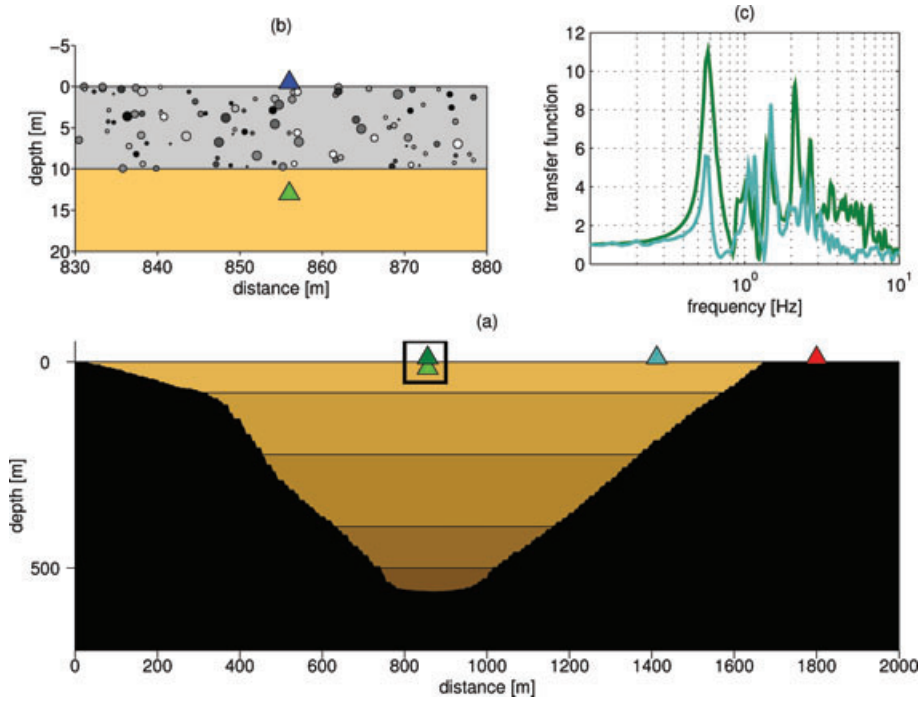

Figure 3. Overview of the different steps used to estimate the non-linear response of the Sion basin. (a) 2-D cross-section for computation of transfer function between valley surface and bedrock. (b) The response of the superficial cohesionless layer is calculated using a fully non-linear 1-D finite difference method. (c) Transfer function between a receiver near the valley centre (darkgreen) or near the basin edge (cyan) and outcropping bedrock.

Table 1. Geophysical parameters of the individual layers in the cross-section (Fig. 3).

z	V_p	V_s	ρ	Q_p	Q_s	Geological interpretation
0–10	800	200	1470	25	25	Non-linear sandlayer
10–75	1500	320	1600	25	25	Deltaic sediments
75–225	1900	480	1900	25	25	Lacustrine deposits
225–400	1900	750	1900	25	25	Glaciolacustrine deposits
400–500	1900	800	1900	25	25	Meltout and reworked till
500–560	2000	900	2000	25	25	Subglacial deposits
0–750	4000	2325	2500	100	100	Bedrock

Notes: Depth ranges z are in m, velocities V in ms^{-1} and densities ρ in kg m^{-3}. Geological characterizations correspond to the interpretation by Pfiffner *et al.* (1997). The uppermost non-linear layer was not used for the DBEM computations.

frequency content of the signal is non-stationary and modelled with a modified ω-square model, which gives the synthetics a realistic frequency content. The method depends on existing strong ground records in a given region and is able to simulate the natural variability observed in real data. Pousse *et al.* (2006) calibrated the model with records from the Japanese K-net accelerometer array.

Syntethics are generated depending on the magnitude, source-site distance and site conditions. To sample different levels of rock ground motion we used magnitudes of 4.0, 4.5, 5.0, 5.5, 6.0 and 6.5 and hypocentral distances of 5, 10, 20 and 40 km. We generated 60 synthetic seismograms for each magnitude–distance combination.

For each of the 1440 generated seismograms, the following steps were performed to compute the non-linear ground motion on the valley surface.

(i) The synthetic seismograms obtained with the method of Pousse *et al.* (2006) are representative for an EC8 soil class A site with $\overline{V_s}(30) > 800$ ms^{-1}, where $\overline{V_s}(30)$ denotes the average shear wave velocity in the top 30 m. In order to obtain signals that are representative of outcropping bedrock with $V_S = 2325$ ms^{-1} (red triangle in Fig. 3a), a deconvolution must be applied on the synthetic seismograms.

Cotton *et al.* (2006) provides a set of generic single parameter rock site models for specific values of $\overline{V_s}(30)$. We selected their velocity model for $\overline{V_s}(30) = 900$ ms^{-1} and used it to deconvolve our synthetics to surface ground motion at a depth of 511 m, where the shear velocity reaches 2325 ms^{-1} in the generic velocity model.

(ii) We compute the transfer function between a receiver near the valley centre and the outcropping rock using the horizontal ground motion obtained from the 2-D DBEM simulations. The ground motion on bedrock is convolved with this complex transfer function (darkgreen line in Fig. 3c). The obtained waveform represents the horizontal ground motion on the surface at the basin centre (darkgreen triangle in Fig. 3a). The same procedure is followed for a receiver near the basin edge (cyan transfer function and triangle in Fig. 3).

(iii) Because the empirical input signal contains a random phase, convolution with the deterministic phase from the DBEM creates in some cases unrealistic seismograms, which exhibit an increasing envelope towards the end of the signal. From visual inspection of the 1440 synthetic seismograms, we rejected signals with unrealistic shapes. 928 signals were left for the remaining processing.

(iv) The signal on the basin surface is deconvolved to obtain the signal in a borehole at 12 m depth (lightgreen triangle in Fig. 3a).

(v) Finally, the signal at the bottom of the soft layer is used as vertically incident SH ground motion for the NOAH finite difference code (Fig. 3b) using borehole boundary conditions. The results represents the acceleration on the surface of the non-linear layer (red triangle in Fig. 3a).

(vi) Response spectra are computed for each signal on the soil surface and the corresponding rock ground motion. The ratio

between the spectral acceleration (SA) on soil and rock is calculated for different frequencies.

This approach allows us to analyse the combined effects of the deep 2-D basin structure and the shallow non-linear layer.

3.2 The strain space multishear mechanism model

The 'NOAH' simulation program (Bonilla *et al.* 2005) is based on the multishear mechanism model introduced by Towhata & Ishihara (1985), which describes the hysteretic behaviour of the stress–strain relationship and the generation of pore pressure. Iai *et al.* (1990a) expanded the model to account for the dilatant nature and cyclic mobility of sands.

In this model the behaviour of sand under the plane strain condition is represented as a relation between effective stress and strain vectors

$$\boldsymbol{\sigma}' = \begin{pmatrix} \sigma'_x \\ \sigma'_y \\ \tau_{xy} \end{pmatrix} \quad \text{and} \quad \boldsymbol{\epsilon} = \begin{pmatrix} \epsilon_x \\ \epsilon_y \\ \gamma_{xy} \end{pmatrix}, \tag{1}$$

where σ_x and σ_y represent normal stress, τ_{xy} represents shear stress and the strain components are given from displacements in u and v directions by

$$\epsilon_x = \frac{\partial u}{\partial x}, \quad \epsilon_y = \frac{\partial v}{\partial y}, \quad \gamma_{xy} = \frac{\partial u}{\partial y} + \frac{\partial v}{\partial x}. \tag{2}$$

The multiple shear mechanism model relates stress and strain through the following incremental equation (Iai *et al.* 1990b)

$$\mathrm{d}\boldsymbol{\sigma}' = K_a \boldsymbol{n}^{(0)} \boldsymbol{n}^{(0)T} (\mathrm{d}\boldsymbol{\epsilon} - \mathrm{d}\boldsymbol{\epsilon}_p) + \sum_{i=1}^{I} R^{(i)}_{L/U} \boldsymbol{n}^{(i)} \boldsymbol{n}^{(i)T} \mathrm{d}\boldsymbol{\epsilon}. \tag{3}$$

The first term ($i = 0$) represents a volumetric mechanism specified with rebound modulus K_a, volumetric strain increment due to dilatancy $d\boldsymbol{\epsilon}_p$ and direction vector $\boldsymbol{n}^{(0)}$

$$\mathrm{d}\boldsymbol{\epsilon}_p = \begin{pmatrix} \frac{\epsilon_p}{2} \\ \frac{\epsilon_p}{2} \\ 0 \end{pmatrix}, \quad \boldsymbol{n}^{(0)} = \begin{pmatrix} 1 \\ 1 \\ 0 \end{pmatrix}. \tag{4}$$

The second term in eq. (3) represents the shear mechanism with the tangent shear modulae $R^{(i)}_{L/U}$. The subindices L and U indicate the loading and unloading processes, respectively, which are defined by the generalized Masing rules. Each mechanism i represents a 1-D shear-stress and shear-strain relation mobilized at angle θ_i given by

$$\theta_i = (i-1)\Delta\theta \quad (\text{for } i = 1, \ldots, I) \quad \text{and} \quad \Delta\theta = \frac{\pi}{I}. \tag{5}$$

The direction vectors $\boldsymbol{n}^{(i)}$ in eq. (3) are defined by

$$\boldsymbol{n}^{(i)} = \begin{pmatrix} \cos\theta_i \\ -\cos\theta_i \\ \sin\theta_i \end{pmatrix}. \tag{6}$$

A detailed explanation of the method can be found in Iai *et al.* (1990a,b).

3.3 Dilatant behaviour soils

By examination of laboratory data, Towhata & Ishihara (1985) found that the pore pressure excess correlates with the cumulative shear work produced during cyclic loading. The model developed by Iai *et al.* (1990a,b) describes this correlation with five 'dilatancy parameters': the parameter w_1 controls overall dilatancy; p_1 the initial and p_2 the final phase of dilatancy; S_1 represents the ultimate limit of dilatancy and c_1 the threshold limit. These parameters are determined by fitting laboratory data from stress-controlled cyclic mobility tests. Details of this constitutive model can be found in Iai *et al.* (1990a,b).

To understand the behaviour of sand during cyclic loading, two different movements of the sand grains must be considered. Weak shearing causes a 'slip-down' movement of sand grains in loose material, which results in a contractive behaviour of the layer. Strong shearing, however, will cause a 'roll-over' movement of sand grains, resulting in a dilatant behaviour of already compressed material. The 'phase transition angle' ϕ_p marks the transition from contractive to dilatant behaviour in a plot of shear-stress versus effective normal stress (Bonilla *et al.* 2005).

3.4 Laboratory tests on soil samples

Several disturbed and undisturbed soil samples were extracted from an excavation pit at a construction site in Visp at 6.3 m depth. The water table has been lowered artificially during construction below the site. For our computations we assume that the soil is fully saturated below the water table at 1.5 m.

From these samples the porosity and density ρ were determined (Table 2). The angle of internal friction ϕ_f was determined to be 39.7° from standard triaxial tests. The phase transformation angle ϕ_p was estimated from the shear resistance angle ϕ (Ishihara & Towhata 1982)

$$\tan(\phi_p) = \frac{5}{8}\tan(\phi). \tag{7}$$

A resonant column test was performed to determine the maximum shear modulus $G_{\max}$ and maximum hysteretic damping $\xi_{\max}$. The largest measured shear wave velocity was 210 ms^{-1} at 200 kPa, which compares well with our results from the ambient noise array measurements (Fig. 2).

Six undrained cyclic triaxial tests with different shear stress were performed up to 5 per cent peak-to-peak shear strain on the same samples to determine the parameters for the cyclic mobility model. A detailed description of all laboratory tests and results can be found in Weber *et al.* (2007).

3.5 Identification of dilatancy parameters

We followed the procedure described in Iai *et al.* (1990a) to identify the dilatancy parameters p_1, p_2, w_1, S_1 and c_1 from the undrained cyclic triaxial tests. First, we plotted the liquefaction resistance curve (Fig. 4), which shows the cyclic shear stress ratio versus the number of cycles required to cause a shear strain of 5 per cent double amplitude, The cyclic shear stress ratio is defined as the applied shear strain τ_{xy} normalized by the initial effective confining pressure σ'_{m0}. For each cyclic test, we plotted the shear stress τ_{xy},

Table 2. Key soil parameters determined from laboratory testing.

Description	Symbol	Value
In situ dry density	ρ_d	1410 kg m^{-3}
In situ porosity	n	49.6 per cent
Shear resistance angle	ϕ	39.7°
Phase transformation angle	ϕ_f	27.4°
Maximum hysteretic damping	$\xi_{\max}$	0.25
Maximum shear velocity	V_s	210 ms^{-1}

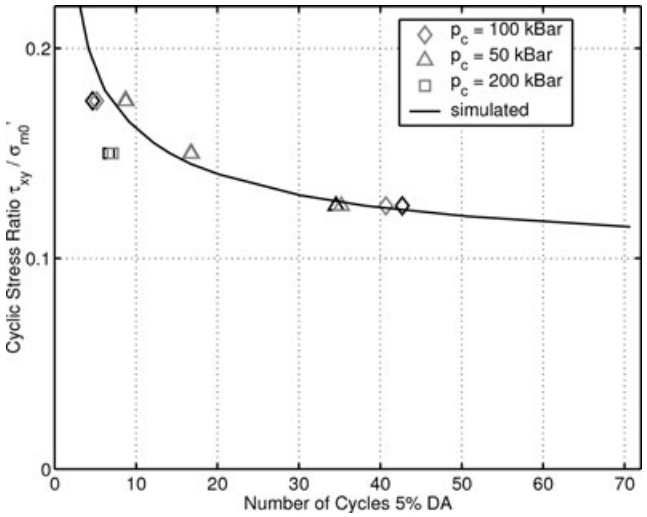

Figure 4. Liquefaction resistance curve. The cyclic shear stress ratio τ_{xy}/σ'_{m0} is plotted as a function of the number of cycles required to cause a shear strain of 5 per cent double amplitude. Grey symbols denote results from the laboratory tests, black symbols results from the simulations. The solid black line shows the synthetic liquefaction resistance curve obtained from the determined dilatancy parameters (Table 3).

the shear strain γ_{xy} and the pore water pressure U as a function of the number of cycles. We determined the dilatancy parameters by fitting the simulated pore water pressure and strain amplitude to the observed values.

Fig. 5 gives an example of observed and simulated cyclic tests. It also shows the stress–strain relationship (τ_{xy} versus γ_{xy}) and the stress path (shear stress τ_{xy} versus effective confining stress σ_m) as well as the effective confining stress σ_m as a function of the cycle number.

Table 3. Dilatancy parameters identified from the six laboratory tests.

	p_1	p_2	w_1	S_1	c_1
Test 4	0.35	0.95	2.00	0.005	1.5
Test 5	0.40	1.05	1.50	0.005	1.5
Test 6	0.39	0.99	1.90	0.005	1.5
Test 7	0.38	0.95	1.55	0.005	1.5
Test 8	0.42	0.98	1.80	0.005	1.5
Test 9	0.40	1.00	1.10	0.005	1.5
Mean	0.39	0.99	1.64	0.005	1.5
S.D.	0.02	0.03	0.30		

The parameter S_1 was set to 0.005 and c_1 to 1.0 as a first guess. Then we estimated p_1 and w_1 from the first part of the pore water generation curves by trial and error. Next the value for p_2 was determined by fitting the amplitude of the shear strain. We performed the analysis for all measured test data and found quite different values for p_1, w_1 and p_2 depending on the analysed data set.

As described in Iai *et al.* (1990a) we increased the value of c_1 by small steps and repeated the analysis for all our test data. Finally, using $c_1 = 1.5$ we found consistent values for p_1, p_2 and w_1 (Table 3).

By computing the mean of these test results we obtained $p_1 = 0.42$, $w_1 = 1.80$ and $p_2 = 0.98$; these values will be used to characterize the non-linear layer in our simulations. Fig. 4 shows the synthetic liquefaction resistance curve obtained with the identified dilatancy parameters.

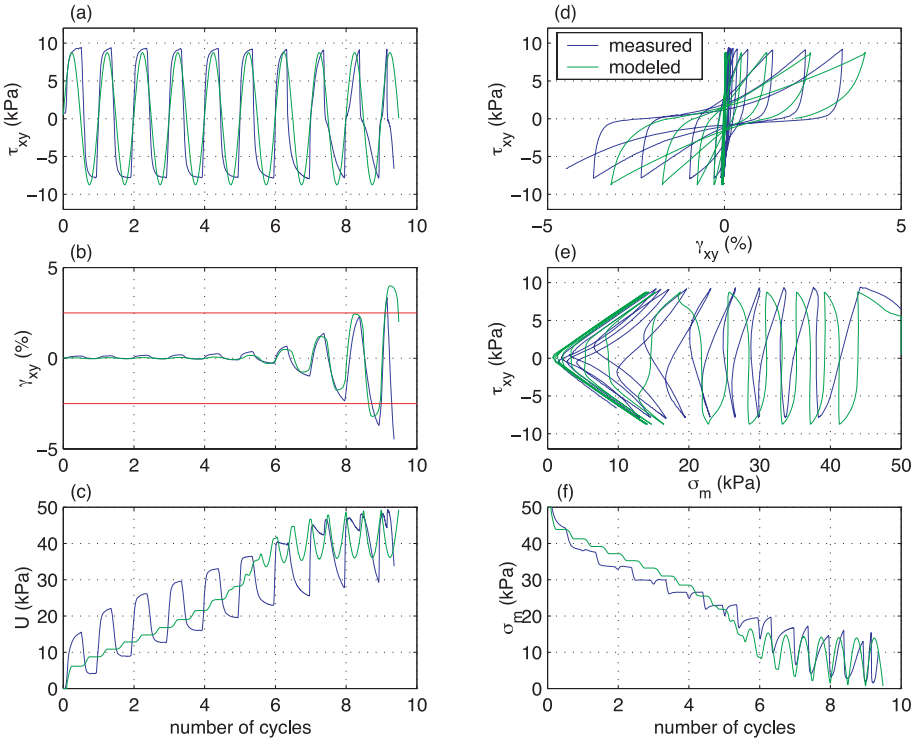

Figure 5. Results of undrained cyclic triaxial test number 8 (blue) on soil samples from Visp. The simulated curves (green) were obtained using $p_1 = 0.42$, $w_1 = 1.80$, $p_2 = 0.98$, $S_1 = 0.005$ and $c_1 = 1.5$ (Table 3). (a) shear stress τ_{xy}, (b) shear strain γ_{xy}, (c) pore water pressure U versus the number of cycles. (d) Shear-stress τ_{xy} versus shear strain γ_{xy}. (e) Stress-path showing shear-stress τ_{xy} versus effective mean stress σ_m. (f) Effective mean stress as a function of the number of cycles.

Table 4. Material properties for the non-linear 1-D simulations.

#	z	σ'_{ma}	V_s	ρ	ϕ	ϕ_p	K_0	$\xi_{\max}$
1	1.5	7.2	200	1470	39.7	–	0.5	0.25
2	10	27.5	200	1470	39.7	27.4	0.5	0.25
3	12	44.5	320	1600	39.7	–	0.5	0.25

Notes: Depths z are in m, velocities V_s in ms^{-1} and densities ρ in kgm^{-3}. σ'_{ma} is the effective mean stress in kPa computed at the middle of each layer. K_0 is the coefficient of earth at rest.

3.6 1-D non-linear simulations

The 1-D non-linear simulation with the 'NOAH' code were run for a 3-layer model (Table 4). The top layer represents the unsaturated soil above the water table, the second layer the saturated non-linear layer and the third layer corresponds to the deltaic sediments in Table 1. The coefficient of earth at rest K_0 represents the horizontal to vertical ratio of the initial effective normal stress. Given the young age of the deposit we assumed that the soil has not yet suffered strong perturbation due to seismic activity. Therefore, we used $K_0 = 0.5$, which corresponds to normal consolidation.

We used a time step dt of 10^{-4} seconds and a spatial step dx of 0.5 m. The simulations were run up to 10 Hz, which corresponds to 40 gridpoints per wavelength. Since the deconvolved signal that served as input represents a simulated borehole record, it served as a dynamic boundary condition in the FD code.

4 SIMULATION RESULTS

We will first analyse the response of the non-linear layer at the valley centre for a few selected events and then analyse the total site response for the complete set of synthetic earthquakes.

4.1 Example of linear soil response

Fig. 6 shows the simulation results for a synthetic M 4.5 event at 40 km epicentral distance. Although the peak ground acceleration

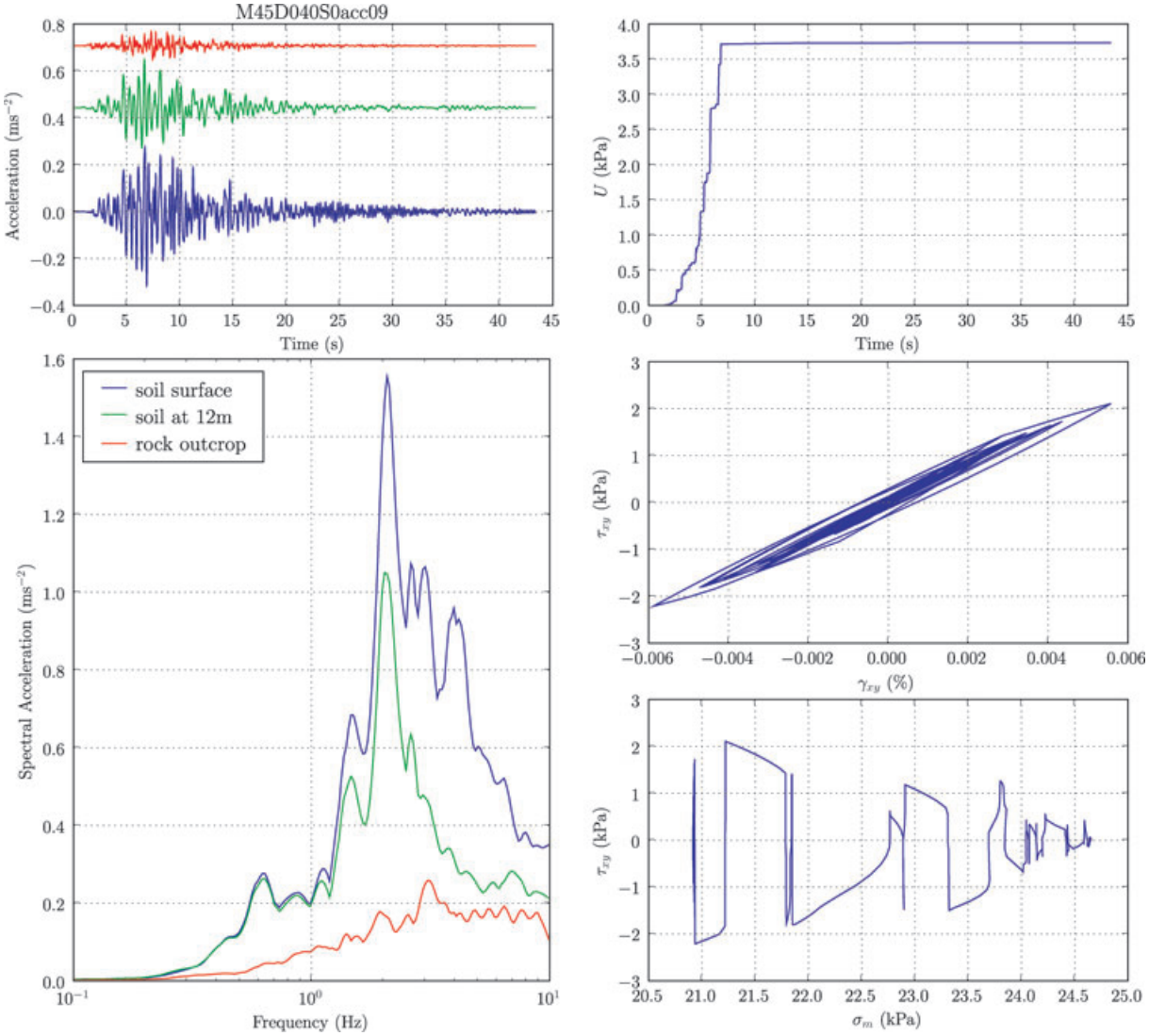

Figure 6. Results of combined 2-D linear and 1-D non-linear simulations for a M 4.5 event at 40 km hypocentral distance. Left-hand panels: acceleration (top panel) and response spectra for 5 per cent damping (bottom panel) representing ground motion on outcropping rock (red), below the non-linear layer (green) and on the soil surface (blue). Right-hand panels: Pore water pressure development (top panel), stress–strain relationship (centre panel) and stress path (effective confining pressure versus stress, bottom panel) in the middle of the layer.

(PGA) on the outcropping rock (red) is less than 0.07 ms^{-2}, the response of the basin amplifies it to more than 0.20 ms^{-2} below the non-linear layer (green). On the surface of the non-linear layer the signal (blue) is further amplified, reaching a peak ground velocity of 0.31 ms^{-2}. We computed response spectra for the signals on the outcropping rock (red), below the non-linear layer (green) and on the surface (blue). Amplification by the deep basin structure creates a significant peak at 2 Hz below the uppermost layer, which is even more dominant on the surface of the low-velocity layer (Fig. 6). Additionally, a peak appears at approximately 5 Hz on the soil surface; this peak represents the resonance frequency of the shallow deposit. The fundamental frequency of the basin at 0.6 Hz is not affected by the uppermost layer. The right-hand column in Fig. 6 shows the development of excess pore water pressure, the stress–strain relation and the stress path. The excess pore water pressure increases quickly after the arrival of the first energetic *S*-wave phases, but it remains well below the confining pressure. The stress–strain relation shows that the soil behaviour is approximately linear for this level of input ground motion. Fig. 7 shows the maximum shear strain, shear stress and pore water pressure as a function of depth for the discussed events.

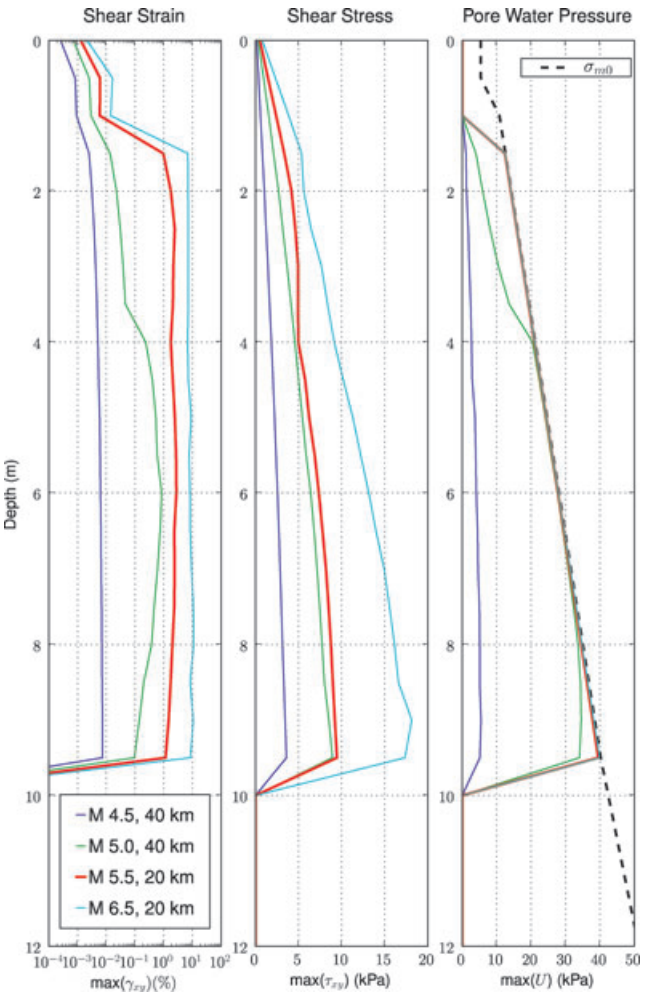

Figure 7. Maximum shear strain, maximum shear stress and maximum pore water pressure as a function of depth for the events shown in Figs 6, 8, 9 and 10. The dashed line in the left-hand plot shows the confining pressure as a function of depth.

4.2 Example of cyclic mobility

Fig. 8 shows an example simulating an *M* 5 event at 40 km hypocentral distance. The first 10 s show a similar amplification as the linear example in Fig. 6. The excess pore water pressure, however, increases very quickly, and almost equals the confining pressure after 10 s. The maximum pore water pressure is close to the confining pressure for depth range between 4 m and the bottom of the soft layer (Fig. 7). Both the stress–strain relation and the stress-path show that the soil enters dilatant behaviour for this weak input ground motion. After approximately 10 s, spiky waveforms appear on the surface accelerogram.

Even though the soil exhibits cyclic mobility, it causes an overall amplification of response spectra at 2 and 5 Hz. Unlike in the linear case, the low-frequency peak caused by the deep basin at 0.6 Hz shows a higher amplitude on the surface than at 12 m depth. This is probably directly related to the triangle-shaped long-period phases in the surface accelerogram (Fig. 8).

4.3 Example of reduced amplification

In Fig. 9, the simulation results for an *M* 5.5 event at 20 km hypocentral distance are shown. In this example, the peak ground motion is 0.5 ms^{-2} on rock and 1.5 ms^{-2} below the non-linear layer. The signal on the surface of the cohesionless soil reaches only 1.1 ms^{-2} PGA and shows the characteristic high-frequency spikes riding on a low-frequency carrier. A comparison of response spectra shows that the non-linear layer causes a reduction of overall amplification, especially at high frequencies. Additionally, the resonance frequencies are shifted to lower values. The pore water pressure increases very quickly and almost equals the confining pressure from the ground water table down to the base of the soft layer (Fig. 7).

4.4 Example of liquefaction

Fig. 10 shows the same analysis for an *M* 6.5 earthquake located 20 km from the site. For this event the peak ground acceleration reaches 3 ms^{-2} below the non-linear layer, though the spikes on the surface reach only 2.1 ms^{-2}. A comparison of response spectra shows that the non-linearity results in an overall de-amplification between rock and soil in the frequency range from 5 to 7 Hz. The deep basin response is shifted towards lower frequencies and reduced in amplitude. The shear strain is consistently exceeding 5 per cent in the saturated part of the non-linear layer (Fig. 7). Liquefaction is not directly implemented in the 'NOAH' program; though if we follow the convention that 5 per cent deformation means failure (e.g. Ishihara 1996), liquefaction does occur for this event.

4.5 Dependency of spectral amplification on input ground motion

We computed spectral ratios from the synthetic ground motion on rock and on the surface of the non-linear layer for all synthetic events. Then we calculated the ratio between SA on the soil surface and on rock for different frequencies. Fig. 11 shows the ratio of SA at the valley centre as a function of rock SA for 0.5, 1, 1.5, 2, 3, 5, 7.5 and 10 Hz as well as PGA (100 Hz). The SA ratios show a great variability at all levels of rock SA, which is a consequence of the complicated response of non-linear soils. To outline the general trend a third-order polynomial was fitted through the data after

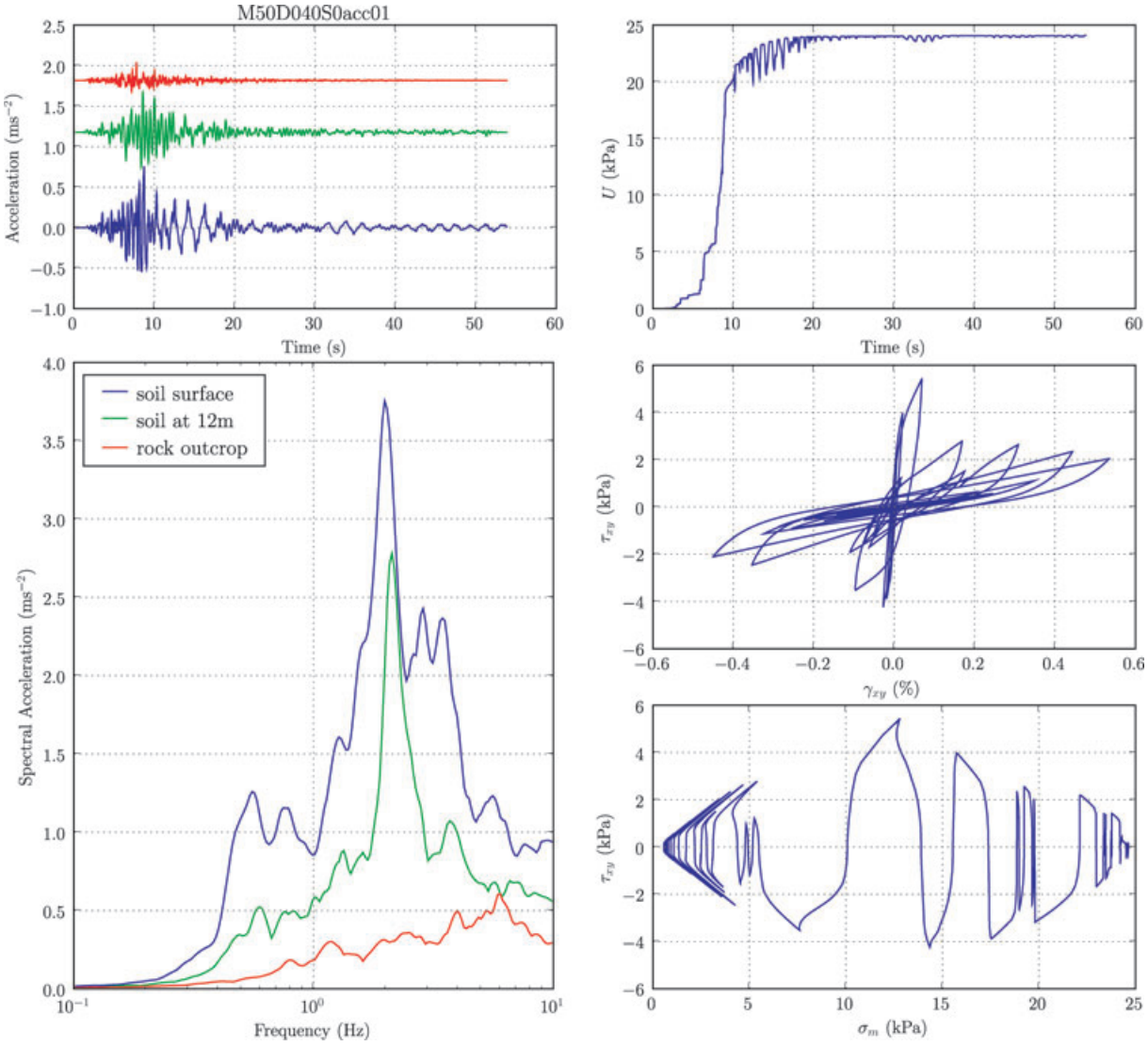

Figure 8. Same as Fig. 6, but for an M 5.0 event at 40 km hypocentral distance.

computing the natural logarithm of the SA on rock and the amplification ratio. At most frequencies, the SA ratio is independent of the rock SA for input SA below 0.10 ms^{-2}, which corresponds to linear soil behaviour. For higher levels of input SA the ratio decreases and eventually drops below unity for rock SA above 2–3 ms^{-2}. This reflects the decreased amplification and de-amplification occurring for high levels of input ground motion. These results suggest that soil non-linearity becomes important for very low levels of input ground motion compared to worldwide observations of non-linearity.

At low frequencies (0.5–2 Hz), the SA ratio is often higher for rock SA of about 0.10 ms^{-2} than for 0.01 ms^{-2}, which is the opposite of the expected behaviour. This suggests that increased amplification may occur at the onset of cyclic mobility before reduced amplification becomes notable. This confirms the earlier observations from the examples shown in Figs 6 and 8, where the low-frequency resonance of the basin was amplified by the uppermost non-linear layer.

Fig. 12 shows the spectral ratios for a receiver near the basin edge as a function of SA on rock. Compared to the valley centre the spectral ratios are generally lower, especially at 0.5 Hz and between 5.0 and 10 Hz. This reflects the differences in the transfer functions of the two receiver positions (Fig. 3c). The differences are more pronounced for low levels of rock SA than for high levels. Non-linearity therefore tends to reduce the differences in site response between the two receiver positions. Near the basin edge reduced amplification becomes appreciable for spectral acceleration exceeding about 0.5 ms^{-2} on rock.

4.6 Absolute spectral accelerations

In Fig. 13, we have plotted the response spectra for 5 per cent damping of the simulated events with magnitudes between 6.0 and 6.5 and with hypocentral distances between 10 and 40 km. Both results for the basin edge and for the valley centre are shown.

For comparison the applicable design spectra SIA261 is shown (Schweizerischer Ingenieur-und Architektenverein 2003). The design spectra was computed for soil type 'D', which is defined as a deposit of unconsolidated fine sands, silts and clays with a thickness of more than 30 m and shear wave velocities between 150 and 300 ms^{-1}.

At the valley centre the design spectra is exceeded during most simulated events at a frequency of approximately 0.5 Hz. This

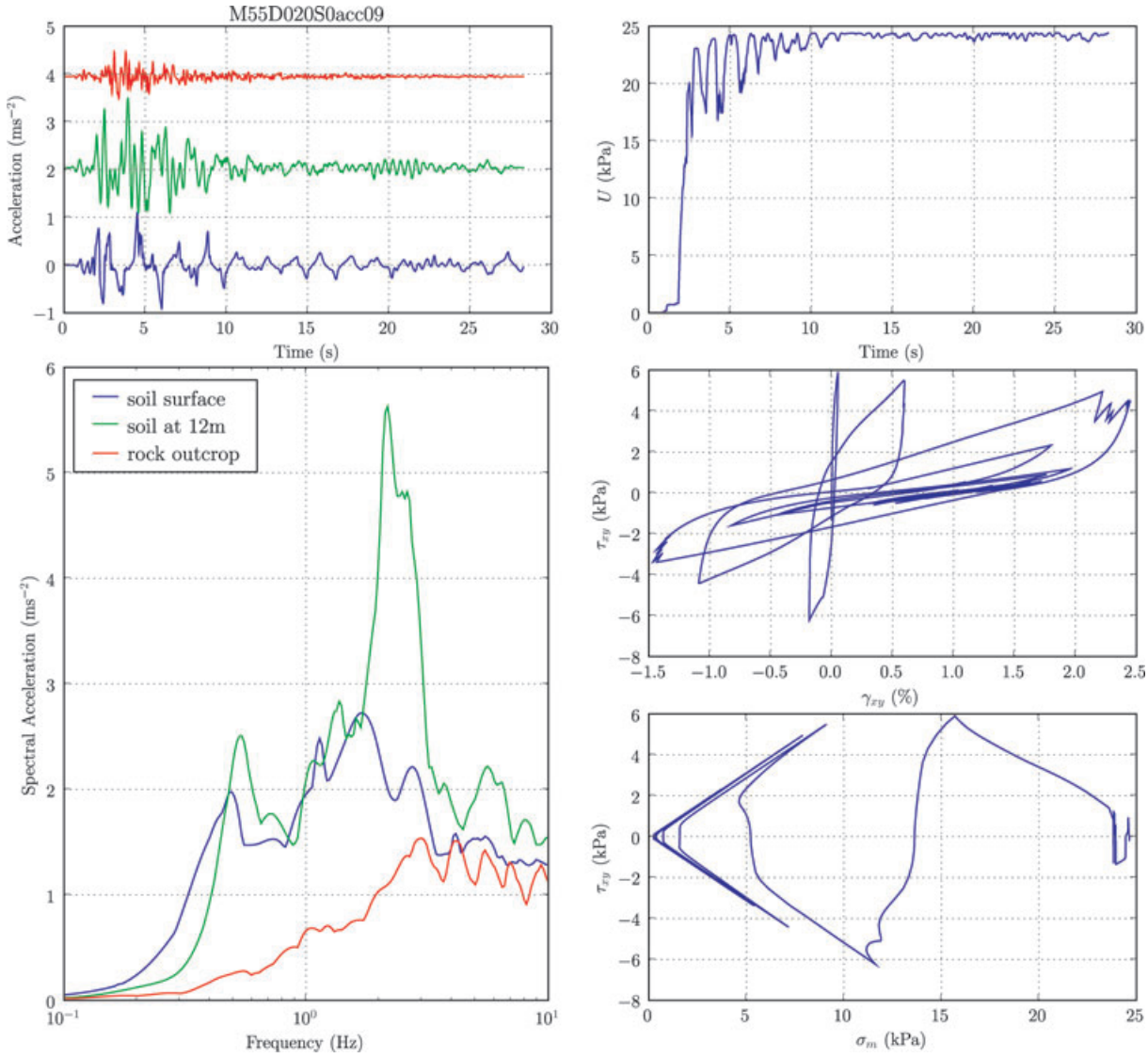

Figure 9. Same as Fig. 8, but for an M 5.5 event at 20 km hypocentral distance.

frequency corresponds to the 2-D resonance frequency of the basin, which is shifted towards lower values by the non-linear behaviour of the uppermost soil. Exceedance of the design spectra by a factor of up to 2 occurs for many simulated events at this frequency. SAs exceeding the design spectra can also be observed for a number of events at about 0.70 Hz. At higher frequencies above 1 Hz the SA of most events remains below the design spectra, and the exceedance amounts to less 30 per cent for the vast majority of the simulated events.

Near the basin edge no significant exceedance of the design spectra occurs at 0.5 Hz, and the SA remains below the norm for the prevailing number of events at higher frequencies.

4.7 Influence of deep basin on non-linear soil behaviour

In order to estimate the influence of the deep basin on the overall analysis of non-linearity we repeated the above calculation without using the transfer function of the 2-D simulation. Instead, the synthetic seismograms obtained by the method of Pousse *et al.* (2006) were deconvolved down to a depth of 12 m and fed directly into the 'NOAH' program as input ground motion. The result represents the ground motion on the surface of a shallow non-linear low-velocity layer overlying a horizontally layered structure.

The black lines in Figs 11 and 12 show the polynomials obtained from these purely 1-D non-linear simulations. As we observed earlier the differences are most pronounced for low levels of input ground motion, and the polynomials obtained from the three different methods tend to coincide for high acceleration levels on rock (Fig. 12).

For frequencies between 0.5 and 2.0 Hz the spectral ratios obtained for the basin edge and the basin centre are generally larger than those obtained for a horizontal structure. At higher frequencies (5.0–10 Hz) the spectral ratios obtained from the 1-D simulations are similar to those obtained for the basin centre, while the amplifications near the basin edge are lower than those of the 1-D simulations for low acceleration levels on rock.

The onset of non-linearity occurs at comparable levels of rock SA for the purely 1-D simulations and the simulations including the basin structure. This implies that the main reason for the early onset of non-linearity is the soil, rather than the influence of the basin. The dilatancy parameters obtained from the cyclic tests show

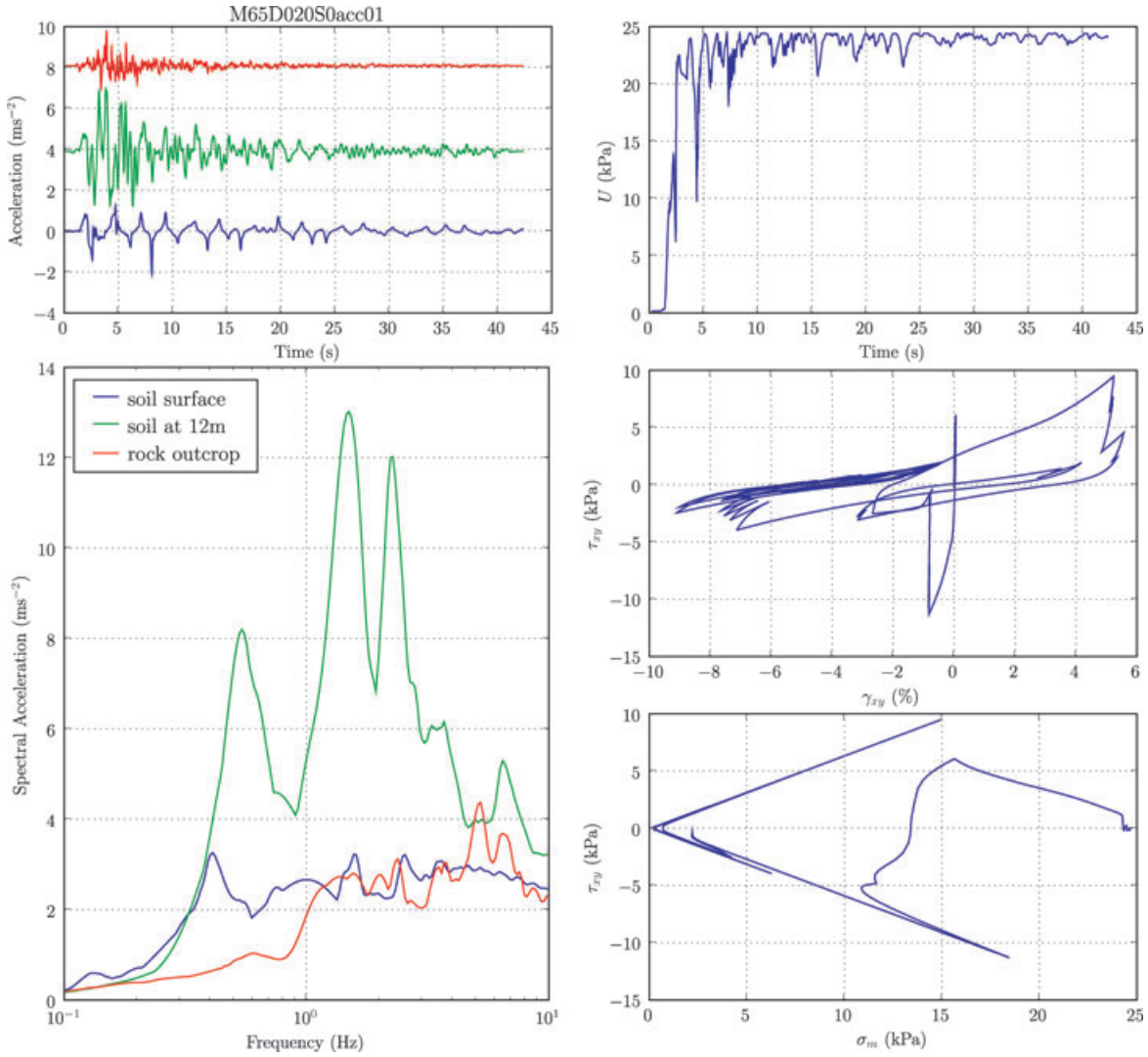

Figure 10. Same as Fig. 8, but for an *M* 6.5 event at 20 km hypocentral distance.

that the soil is very weak, which is reflected by the strong impact of cyclic mobility in our simulations.

4.8 Evaluation of liquefaction potential

To estimate the importance of soil liquefaction we evaluated the maximum strain encountered in the simulated scenarios. For each magnitude–distance combination, we determined the number of events for which liquefaction would be triggered in the midpoint of the liquefiable layer according to the 5 per cent strain convention, and divided it by the total number of events simulated for the same magnitude–distance combination. Fig. 14(a) shows a contour plot with the occurrence of 5 per cent strain or more as a function of magnitude and distance for the basin centre and the basin edge. It must be emphasized that the resulting liquefaction probabilities are only accounting for the variability of the simulated input ground motion, not the uncertainties in soil parameters at the site.

For the basin centre (Fig. 14, left-hand panel) our simulations indicate that liquefaction may occur at rather large hypocentral distances for a given magnitude, for example, in 10 per cent of the cases at 20 km hypocentral distance for an *M* 5.5 event.

For comparison we are considering two empirical relations that estimate the limiting epicentral distance of sites at which liquefaction has been observed as a function of moment magnitude for shallow earthquakes. Since the synthetic earthquakes generated for this study are based on the hypocentral distance we used the Joyner–Boore distance (Joyner & Boore 1981) assuming a depth of 5 km to evaluate the empirical relations.

Fig. 14 (left-hand panel) compares the liquefaction occurrence obtained from our analysis with empirical relations from Ambraseys (1988) and Papadopulous & Lefkopoulos (1993). The results for the valley centre are yielding soil liquefaction at distances well above those provided by the empirical relations. Given an *M* 5.5 earthquake, for example, our simulations generated soil liquefaction in 10 per cent of the cases at a hypocentral distance of 20 km. The empirical relations by Ambraseys (1988) and Papadopulous & Lefkopoulos (1993) yield a limiting distance of 8 and 12 km, respectively, for an *M* 5.5 event.

The results for the basin edge (Fig. 14, right-hand panel), however, are in agreement with the distance limits computed from the empirical relations, and liquefaction is only triggered at distances below the empirical threshold. This suggests that the strong amplification of the incident wavefield at the basin centre extends the radius within which liquefaction must be expected.

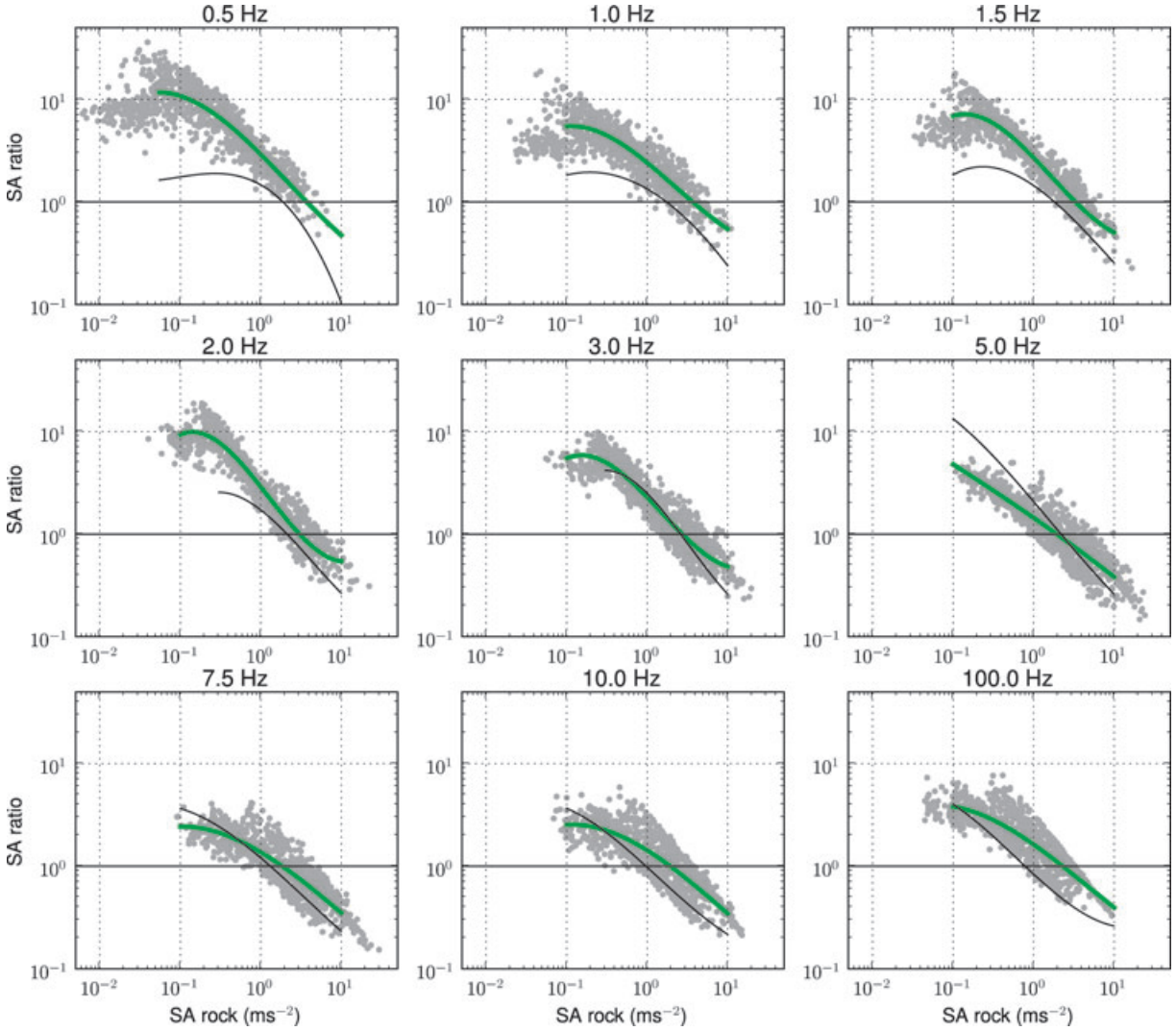

Figure 11. Ratio between spectral acceleration on the surface at the valley centre and rock as a function of spectral acceleration on rock for different frequencies and peak ground acceleration (100 Hz). The green lines show third-order polynomials fitted through the logarithm of the ratios. The thin black lines shows the fit obtained from 1-D non-linear simulations neglecting the 2-D basin.

5 DISCUSSION

5.1 Historical reports of liquefaction

After the 1855 M 6.4 earthquake of Visp, a number of surface changes on soft soil were observed that may be related to liquefaction (Fritsche *et al.* 2006). Sources reported subsidence of farmland below the Rhône level, wavelike structures on previously even soil and wide cracks in the ground. The exact position of these observations is not known, though they were made in the vicinity of our sampling location in Visp.

The epicentre of the 1855 main shock was located approximately 7 km from Visp. Using the macroscopically determined depth of 12 km, this places the sites at about 14 km hypocentral distance. Considering the liquefaction occurrence in Fig. 14 (left-hand panel) for this magnitude and distance, it is very realistic that liquefaction did occur during this event, because it happened in 90 per cent of the simulated scenarios at the valley centre. Even for the simulations near the basin edge (Fig. 14, right-hand panel) liquefaction occurred in 40 per cent of the cases for a magnitude of 6.4 at 14 km hypocentral distance. However, we must keep in mind that these liquefaction occurrences may not be accurate for Visp, because they were computed with the transfer function of the Sion basin.

5.2 Effect of non-linearity on long-period basin response

Non-linearity is generally considered to affect only higher frequencies (>1 Hz), because increased damping effects caused by non-linearity are less influential at low frequencies, and because the layer that exhibits non-linear properties is usually shallow. More specifically, if the seismic response of a soft soil deposit changes due to non-linearity, one would expect that only frequencies equal or higher than the natural frequency of the non-linear layer are affected.

In our case, the resonance frequency of the liquefiable layer

$$f_0 = \frac{V_s}{4h} \tag{8}$$

will be near 5 Hz using $V_s = 200$ ms^{-1} and $h = 10$ m. Even though this value will decrease as the shear-modulus of the material

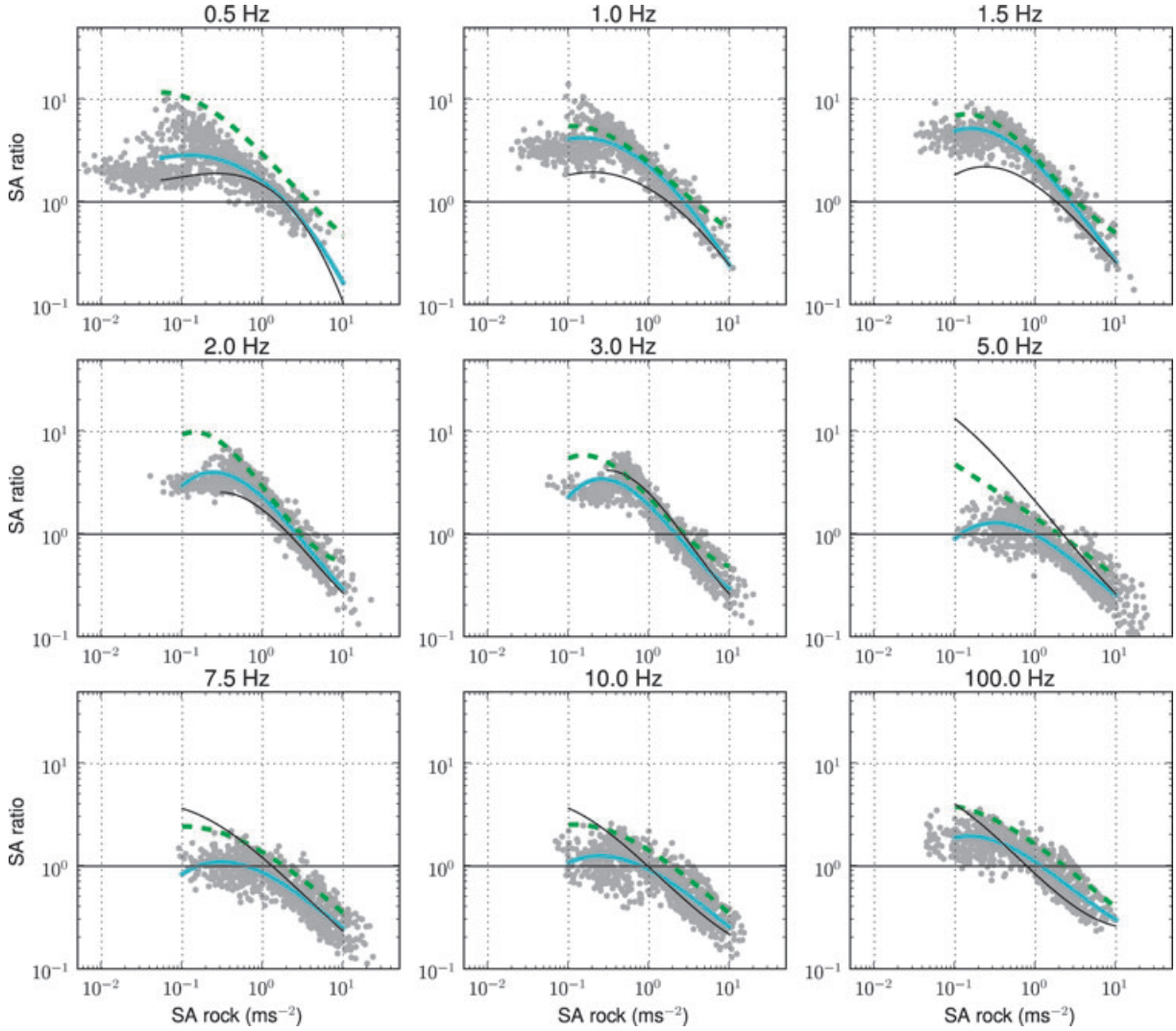

Figure 12. Same as Fig. 11, but for a receiver near the basin edge. Cyan lines show the third-order polynomials fitted through the ratios; the polynomials for the valley centre are given by darkgreen dashed lines.

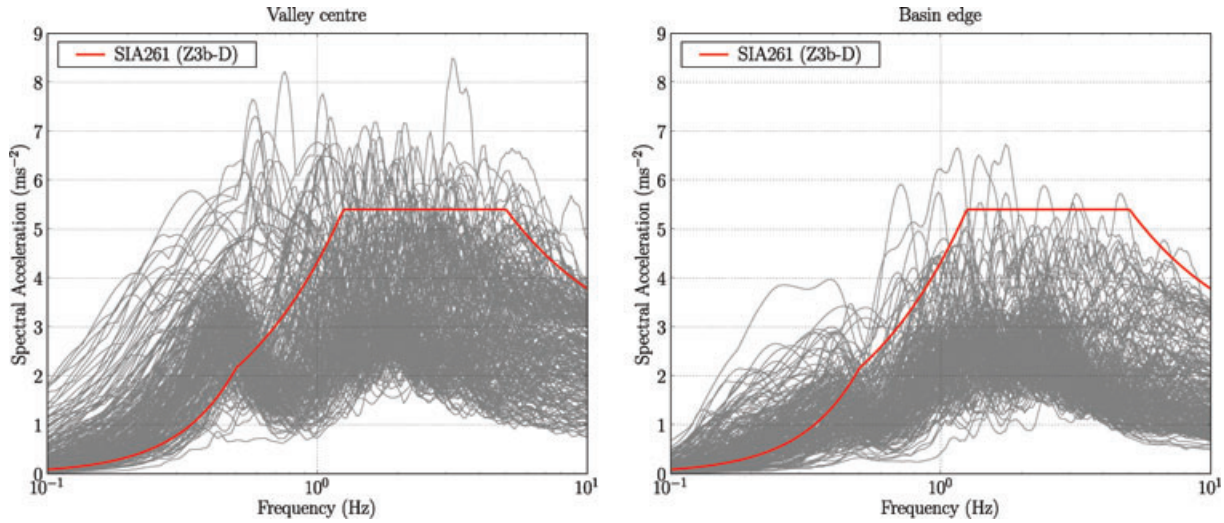

Figure 13. Absolute response spectra of all simulated events with magnitudes between 6.0 and 6.5 and hypocentral distances between 10 and 40 km. The red line shows the design spectra of the norm SIA261 for soil type 'D' (Schweizerischer Ingenieur-und Architektenverein 2003).

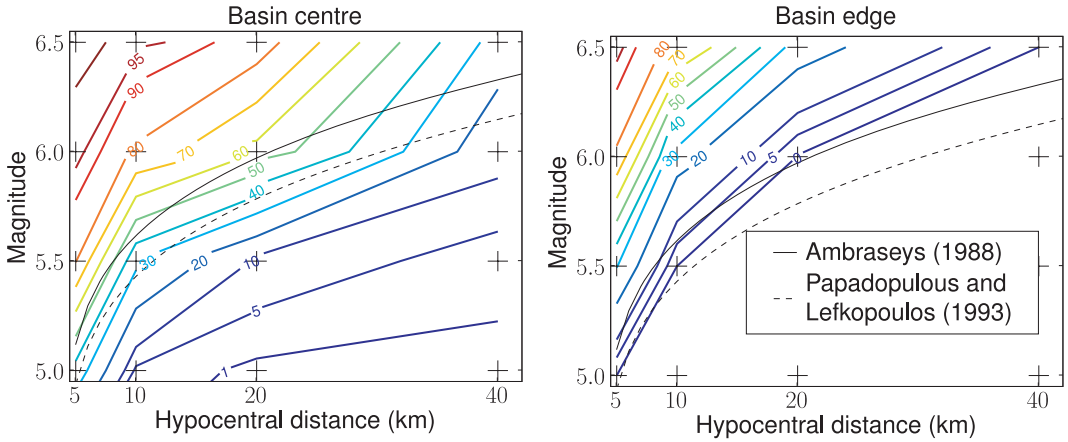

Figure 14. Occurrence of liquefaction (per cent) as a function of hypocentral distance and magnitude for the valley centre (left-hand panel) and the basin edge (right-hand panel). For comparison two empirical relations are shown.

decreases during cyclic loading, it is well above the deep resonance frequency of the basin near 0.5 Hz.

However, our results predict that reduced amplification due to non-linearity will also reduce the site-response at frequencies as low as 0.5 Hz (Figs 11 and 12). Fig. 10 shows how the amplitude of the deep basin response is reduced near the surface and shifted towards lower frequencies. This suggests that the shallow non-linear layer also attenuates waves with periods longer than its natural period, and acts as a cushion between the deeper layers and the surface.

Evidence for this type of decoupling of the free surface from the deeper structure by liquefying soil deposits has been observed during actual earthquakes. After the 1999 İzmit earthquake, for example, Bakir *et al.* (2002) observed that five-to-six storey buildings located on non-liquefiable soil suffered frequent damage or collapse, and the alluvial basin was found to amplify the ground motion near the fundamental periods of the affected buildings (0.25–0.6 s). Structures located on liquefied soil layers, however, suffered no major structural damage, even though they experienced foundation displacements. Bakir *et al.* (2002) concluded that 'liquefied soil layers serve as passive base isolation devices that do not transmit seismic inertial forces to the super-structure under earthquake base excitation'. Our results suggest that this effect will also reduce the site response at frequencies below 1 Hz, even though soil liquefaction is not directly implemented in the soil model used for this study.

5.3 Effect of deep valley resonance on liquefaction

It is likely that long-period excitation of the non-linear layer is important for liquefaction, since the differences between the basin centre and the basin edge are most pronounced at low frequencies (Fig. 12). Fig. 15 compares simulated accelerations at the valley centre with accelerations for the basin edge for an M 6.5 event at 40 km hypocentral distance (example discussed in Section 4.4).

The acceleration time-series below the interface seem quite similar for the basin centre and the basin edge (Fig. 15, top panel). However, the input ground motion at the basin centre carries 16 times more energy at 0.6 Hz than the input ground motion near the basin edge. This is related to the deep 2-D resonance of the basin, which produces the highest amplification in the central part of the valley.

On the surface of the soft soil sharp spikes appear in the accelerogram at the valley centre, which are not present near the basin edge (Fig. 15, bottom panel). These peaks represent the highest acceleration and are related to the maximum strain. Similar to observations made for Kushiro Port (Iai *et al.* 1995; Bonilla *et al.* 2005), the high-frequency spikes are riding on a low-frequency carrier. In our case, the low-frequency carrier corresponds to the deep basin response at 0.6 Hz, which is still very dominant on the surface of the non-linear layer, and shifted slightly towards lower frequencies (Fig. 15, bottom panel). In the example in Fig. 15 the maximum strain reaches 9 per cent at the valley centre, but only 4 per cent near the basin edge. This shows that the frequent occurrence of liquefaction near the valley centre (Fig. 14) can be attributed to the strong long-period amplification.

The divergence between the simulated liquefaction occurrence in the valley centre and the empirical relations for limiting distances (Fig. 14) could partly be related to the simplifications introduced in this study, such as the assumption that only the uppermost layer will exhibit non-linear behaviour. Array measurements of ambient noise in the Sion area reveal a further layer of about 40 m thickness with $V_s \approx 320$ ms^{-1} (Roten *et al.* 2008) below the uppermost 10 m layer. We have not included this layer in the non-linear computation because its dilatancy parameters are unknown. But if this layer did exhibit non-linear behaviour we would typically expect it to be more liquefaction resistant than the uppermost layer, but nevertheless introduce additional damping of the incident wavefield. Since the high-amplitude incident wavefield is responsible for the high occurrence of liquefaction in the valley centre, this additional layer could limit the radius within which liquefaction occurs.

We tested this hypothesis by rerunning the non-linear simulations for the valley centre using a second non-linear layer of 40 m thickness with the same dilatancy parameters as the first layer. The shear-velocity of this layer was set to 320 ms^{-1} and the shear resistance angle ϕ to 45°. The resulting liquefaction occurrence is shown in Fig. 16. We find that using the 50 m model significantly limits the number of cases that exceed the 5 per cent strain threshold in the midpoint of the top layer. While the limiting hypocentral distances predicted by Ambraseys (1988) are still exceeded for some magnitude–distance combinations (e.g. for an M 5.5 event at 10 km distance), the limiting distances after Papadopulous & Lefkopoulos (1993) are not exceeded by the simulated results. This shows that the liquefaction occurrence is sensitive to the number of non-linear layers involved.

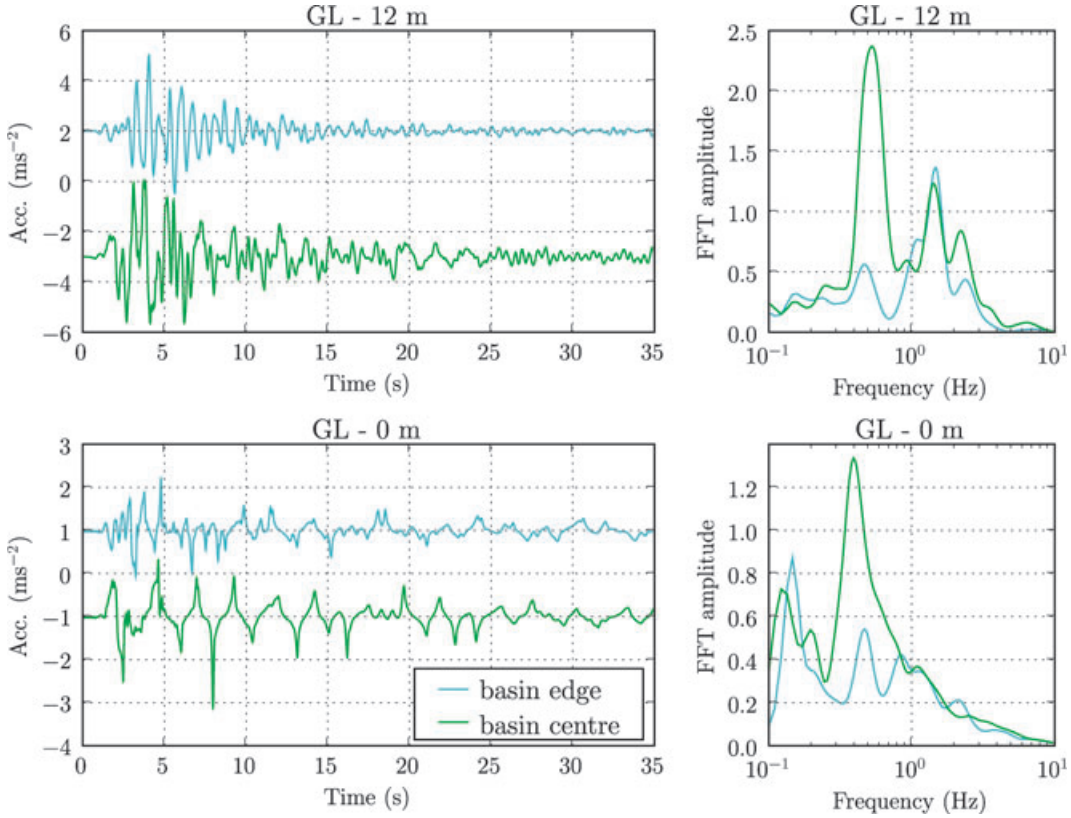

Figure 15. Comparison between simulated ground motion near the basin edge (cyan) and near the basin surface (darkgreen). Acceleration time-series (left-hand panels) and FFT amplitudes (right-hand panels) are shown at 12 m depth (top panel) and on the surface (bottom panel).

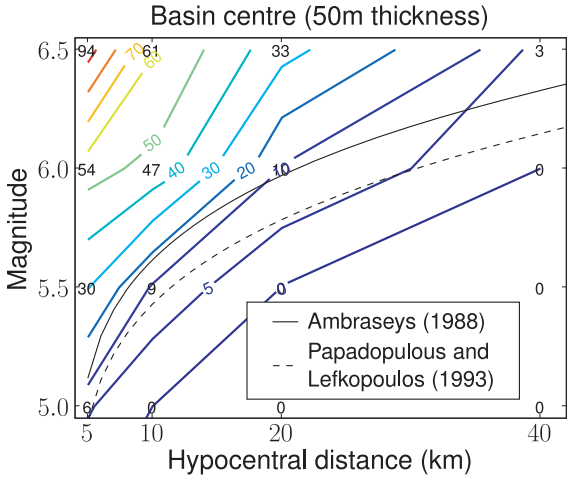

Figure 16. Same as Fig. 14 (left-hand panel), but using two non-linear layers of 50 m total thickness.

5.4 Onset of non-linearity

We found that reduced amplification due to non-linear soil behaviour can be expected at peak ground velocities exceeding 0.5 ms^{-2} (Figs 11 and 12). Beresnev & Wen (1996) compiled a set of worldwide field seismological observations and concluded that non-linearity can be appreciated for rock accelerations above 1–2 ms^{-2}, which is clearly higher than the level of 0.5 ms^{-2} found in this study. However, Beresnev & Wen (1996) also concluded that soil appears to behave slightly more non-linear under laboratory conditions than in nature. This implies that the threshold PGA of 0.5 ms^{-2} may be shifted towards higher values during an actual earthquake.

Hartzell *et al.* (2004) predicted non-linear soil effects using different models, including the model 'NOAHB' which is very similar to the code used in this study. The lowest level of input ground motion they considered is 1 ms^{-2} (∼0.1 g), and they found a reduction in site response by a factor of about 3 compared to the linear response at 3 Hz for a NHRP class E site and a water table of 2.5 m (fig. 5 in Hartzell *et al.* 2004). Considering the curves fitted through our data at 3 Hz (Figs 11 and 12) we find that the site response is reduced by factors between approximately 1.8 and 3.0 at a rock PGA of 1 ms^{-2}. Hartzell *et al.* (2004) did not determine a threshold PGA above which non-linear soil response becomes notable for this soil class, but this comparison shows that our results are generally in line with previous findings obtained with the strain-space-multishear mechanism model.

5.5 Limitations

Certainly this study is based on a number of assumptions and there are some limitations. We assumed that only the uppermost layer will exhibit non-linear response, and that the whole remainder of the sedimentary fill can be described as linear. No soil samples of the lower sedimentary layers are available which would be required to determine the dilatancy parameters. Since both shear wave velocities obtained from ambient noise and boreholes show that the uppermost layer differs from the deeper deposit, extrapolation of the available dilatancy parameters to greater depth would not represent a reasonable option. However, the test we performed in Section 5.3 with the 50 m non-linear model indicates that the occurrence of

liquefaction may be reduced in the presence of additional non-linear layers.

The empirical relation used for the synthetic input seismograms is based on observations including sites that exhibit strong 2-D and 3-D effects, similar to the Rhône basin. Since these signals were deconvolved using 1-D response only and then the 2-D response was added, it is possible that this approach overestimates the input ground motion at the bottom of the non-linear layer. Another shortcoming is that the model of Pousse *et al.* (2006) was calibrated using Japanese strong-motion records, which may not be representative for Swiss rock sites. More accurate results could be obtained with a deterministic approach, though this would require knowledge of location, magnitude and rupture details of possible future earthquakes.

Finally, the soil samples extracted from one location site may not be representative for the whole Rhône valley. To fully assess the impact of non-linearity more laboratory tests with samples from different locations would be needed.

The parameter of earth at rest K_0 is not well constrained. We assumed normal consolidation because the soil is rather young, though we do not know to what extent is has already been perturbed by seismic activity. A higher value of K_0 would increase the strength of the material and reduce the non-linear effects.

6 SUMMARY AND CONCLUSIONS

We have analysed non-linear soil response in the Rhône valley by convolving empirical input ground motion with the 2-D linear valley response and propagating it through a non-linear layer using the 1-D FD program 'NOAH'. The dilatancy parameters that are required for the non-linear simulations were obtained from fitting of laboratory data and show that the soil is rather weak.

The simulation results suggest that soil non-linearity becomes appreciable at SA levels as low as 0.5 ms^{-2} on rock (Fig. 11). At low frequencies (<2 Hz), the onset of cyclic mobility may cause an increase in overall amplification compared to the linear case. With increasing intensity of input ground motion the amplification between rock and soil surface decreases, and de-amplification occurs at rock SAs exceeding approximately 2 ms^{-2}. For most simulated events the absolute SA remains below the design spectra for frequencies above 1 Hz. Only near the valley centre the norm is generally exceeded at frequencies of about 0.5 Hz.

However, it is important to note that strong non-linear effects are very likely to occur at high levels of input ground motion. Fig. 17 shows the strain level at 4.5 m depth near the valley centre as a function of peak ground acceleration on rock. Although the relation exhibits a strong variability, the liquefaction criterion of 5 per cent strain is exceeded by a prevailing number of events for rock PGA above 2 ms^{-2}.

Evaluation of the liquefaction occurrence for specific magnitudes implies that soil failure may occur at distances exceeding those predicted by empirical relations at the valley centre. Near the basin edge, however, the simulated liquefaction occurrence agrees with the empirical relation. We suggested that amplification of long-period ground motion by the deep basin response may provide the low-frequency carrier for the high-frequency spikes, which create the largest acceleration and, therefore, provide the necessary strain to trigger liquefaction. This shows that the response of the whole structure needs to be simulated in order to estimate the importance of non-linear soil behaviour.

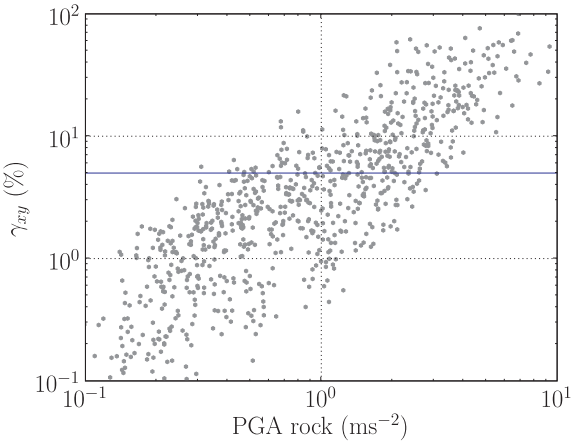

Figure 17. Strain γ_{xy} (per cent) at 4.5 m depth as a function of PGA on rock for the valley centre.

To isolate the impact of the 2-D basin structure we repeated all the simulations using only the 1-D non-linear method. Results of these 1-D non-linear simulations differ from the combined simulations especially at low frequencies, though they are producing cyclic mobility at similarly low levels of input ground motion. This suggests that the strong dilatant nature of the sampled soil, rather than the 2-D basin effect, is responsible for the early onset of non-linearity. We observed that non-linearity reduces the differences in spectral ratios between the basin centre, the basin edge and the horizontally layered velocity model at high levels of ground motion on bedrock.

In this study, we used a simplified approach and we treated wave propagation in non-linear media only in one dimension. The disadvantage of this method is that effects of non-linearity on 2-D and 3-D phenomena such as edge-generated surface waves are neglected.

The results of this study suggest that non-linear soil behaviour is an important factor in the analysis of site effects in the Rhône valley. Results of the simulations confirm that non-linearity is not just reducing the amplification between soil and bedrock in all cases, but more complicated phenomena may develop which impose additional hazard. Spiky waveforms due to partial strength recovery (Bonilla *et al.* 2005) evolved in many simulated scenarios, and it seems that this effect increases the amplification for low levels of input ground motion (Fig. 8). Soil liquefaction poses a significant threat to structures, and our simulation suggest that liquefaction may occur before de-amplification.

However, more soil samples and simulations are needed to analyse the importance of non-linear site response for the whole Rhône basin. Since our results suggest that cyclic mobility will occur for rather low levels of input ground motion, records of moderate local earthquakes on a vertical array, with accelerometers and piezometers at different depths and on the surface, would allow to reject or confirm these findings.

ACKNOWLEDGMENTS

This research was enabled by the following research contracts: project SHAKE-VAL, funded by the Swiss National Science Foundation (No. 200021-101920 and 200020-109177) and the CCES-project COGEAR ('Coupled seismogenic Geohazards in Alpine Regions') funded by the Swiss Federal Institute of Technology. We

would like to thank John Douglas and an anonymous reviewer for their valuable comments that helped to improve the manuscript.

REFERENCES

Álvarez-Rubio, S., Benito, J.J., Sánchez-Sesma, F.J. & Alarcón, E., 2004. The direct boundary element method: 2D site effects assessment on laterally varying layered media (methodology), *Soil Dyn. Earthq. Eng.,* **24,** 167–180.

Álvarez-Rubio, S., Sánchez-Sesma, F.J., Benito, J.J. & Alarcón, E., 2005. The use of direct boundary element method for gaining insight into complex seismic response, *Comput. Struct.,* **83,** 821–835.

Ambraseys, N.N., 1988. Engineering seismology, *Earthq. Eng. Struct. Dyn.,* **17,** 1–105.

Bakir, B.S., Sucuoğlu, H. & Y lmaz, T., 2002. An overview of local site effects and the associated building damage in Adapazar during the 17 August 1999 İzmit earthquake, *Bull. seism. Soc. Am.,* **92**(1), 509–526.

Beresnev, I.A. & Wen, K.-L., 1996. Nonlinear soil response—a reality? *Bull. seism. Soc. Am.,* **86**(6), 1964–1978.

Besson, O., Marchant, R., Pugin, A. & Rouiller, J.-D., 1993. Campagne de sismique-réflexion dans la vallée du Rhône entre Sion et St. Maurice: perspectives d'exploitation géothermique des dépôts torrentiels sous-glaciaires, *Bull. du Centre d'hydrogéologie de l'Université de Neuchâtel,* **12,** 39–58.

Bonilla, L.F., Archuleta, R.J. & Lavallee, D., 2005. Hysteretic and Dilatant behavior of cohesionless soils and their effects on nonlinear site response: field data observations and modeling, *Bull. seism. Soc. Am.,* **95**(6), 2373–2395.

Cotton, Fabrice, Scherbaum, F., Bommer, J. & Bungum, H., 2006. Criteria for selecting and adjusting ground-motion models for specific target regions: application to Central Europe and rock sites, *J. Seismol.,* **10,** 137–156.

Darragh, R.B. & Shakal, A.F., 1991. The site response of two rock and soil station pairs to strong and weak ground motion, *Bull. seism. Soc. Am.,* **81,** 1885–1899.

Field, E.H., Johnson, P.A., Beresnev, I.A. & Zeng, Yu., 1997. Nonlinear ground-motion amplification by sediments during the 1994 Northridge earthquake, *Nature,* **390,** 599–602.

Fritsche, S., Fäh, D., Gisler, M. & Giardini, D., 2006. Reconstructing the damage field of the 1855 earthquake in Switzerland: historical investigations on a well-documented event, *Geophys. J. Int.,* **166**(2), 719–731.

Hartzell, S., Bonilla, L.F. & Williams, R.A., 2004. Prediction of nonlinear soil effects, *Bull. seism. Soc. Am.,* **94**(5), 1609–1629.

Holzer, T.L., Youd, T.L. & Hanks, T.C., 1989. Dynamics of liquefaction during the 1987 Superstation Hills, California, Earthquake, *Science,* **244**(4900), 56–59.

Iai, S., Matsunaga, Y. & Kameoka, T., 1990a. Parameter identification for a cyclic mobility model, *Report of the Port and Harbour Research Institute,* **29,** 57–83.

Iai, S., Matsunaga, Y. & Kameoka, T., 1990b. Strain space plasticity model for cyclic mobility, *Report of the Port and Harbour Research Institute,* **29,** 27–56.

Iai, S., Morita, T., Kameoka, T., Matsunaga, Y. & Abiko, K., 1995. Response of a dense sand deposit during 1993 Kushiro-Oki Earthquake, *Soils Found.,* **35,** 115–131.

Ishihara, K., 1996. *Soil Behaviour in Earthquake Geotechnics,* Clarenton Press, Oxford.

Ishihara, K. & Towhata, I., 1982. Dynamic response analysis of level ground based on the effective stress method, in *Soil Mechanics—Transient and Cyclic Loads,* eds Pande, G.N. & Zienkiewicz, O.C., John Wiley & Sons, Chichester.

Joyner, W.B. & Boore, D.M., 1981. Peak horizontal acceleration and velocity from strong-motion records including records from the 1979 Imperial Valley, California, earthquake, *Bull. seism. Soc. Am.,* **71**(6), 2011–2038.

Papadopulous, G.A. & Lefkopoulos, G., 1993. Magnitude-distance relations for liquefaction in soil from earthquakes, *Bull. seism. Soc. Am.,* **83**(3), 925–938.

Pfiffner, O.A., Heitzmann, S., Mueller, S. & Steck, A., 1997. Incision and backfilling of Alpine valleys: Pliocene, Pleistocene and Holocene processes, *Deep Structure of the Swiss Alps—results of NRP,* Birkhäuser, Basel, pp. 265–276.

Pousse, G., Bonilla, L.F., Cotton, F. & Margerin, L., 2006. Nonstationary stochastic simulation of strong ground motion time histories including natural variability: application to the K-Net Japanese database, *Bull. seism. Soc. Am.,* **96**(6), 2103–2117.

Rosselli, A., 2001, Modélisation gravimétrique bi- et tridimensionelle du substratum rocheux des vallées alpines, *PhD thesis*, Université de Lausanne.

Roten, D. & Fäh, D., 2007. A combined inversion of Rayleigh wave dispersion and 2-D resonance frequencies, *Geophys. J. Int.,* **168,** 1261–1275.

Roten, D., Cornou, C., Fäh, D. & Giardini, D., 2006. Two-dimensional resonances in Alpine valleys identified from ambient vibration wavefields, *Geophys. J. Int.,* **165,** 889–905.

Roten, D., Fäh, D., Olsen, K.B. & Giardini, D., 2008. A comparison of observed and simulated site response in the Rhône valley, *Geophys. J. Int.,* **173,** 958–978.

Sabetta, F. & Pugliese, A., 1996. Estimation of response spectra and simulation of nonstationary earthquake ground motions, *Bull. seism. Soc. Am.,* **86**(2), 337–352.

Schweizerischer Ingenieur-und Architektenverein, Zürich., 2003. *Einwirkungen auf Tragwerke*. Schweizer Norm–SN; 505 261, Bauwesen.

Towhata, I. & Ishihara, K., 1985. Modeling soil behavior under principal axes rotation, in *Fifth International Conference on Numerical Methods in Geomechanics,* Nagoya, Japan, pp. 523–530.

Wathelet, M., Jongmans, D. & Ohrnberger, M., 2004. Surface wave inversion using a direct search algorithm and its application to ambient vibration measurements, *Near Surface Geophys.,* **2,** 211–221.

Weber, T., Laue, J. & Springmann, S.M., 2007. Geotechnical laboratory tests for identification of soil parameters for the cyclic mobility model of sandy soil from Visp (VS), Project report—SHAKE-VAL 2. ETH Zürich, Institute for Geotechnical Engineering.

Wen, K.-L., Beresnev, I.A. & Yeh, Y.T., 1994. Non-linear soil amplification inferred from downhole strong seismic motion data, *Geophys. Res. Lett.,* **21**(24), 2626–2628.